The Structural Analysis of Protein Kinases from *Trypanosoma* and *Leishmania* Parasites

Daayum Mohsin

202113882

Supervisor: Dr Martin Wiese

A thesis submitted in partial fulfilment for the degree of BSc (Hons) in Immunology and Pharmacology. This report is entirely my own work. Any information taken from others has been declared and referenced in the text.

Word count: 4953

Strathclyde Institute of Pharmacy and Biomedical Sciences, University of Strathclyde,

Glasgow G4 0RE.

March 2025

Signed: Date: 3RD March 2025

CONTENTS

Word Count: 4951

Introduction: 1332

Methods: 851

Results: 1219

Discussion: 1551

1 Acknowledgements

I would like to extend my sincere appreciation to my supervisor, Dr. Martin Wiese, whose guidance, expertise, and unwavering support have been critical to the progress and completion of this project. His insightful feedback helped shape the direction of my research and provided the confidence needed to tackle new challenges.

I am also grateful to the lecturers and colleagues at the Strathclyde Institute of Pharmacy and Biomedical Sciences for their helpful discussions and insights regarding bioinformatics and structural analysis. Their willingness to share their expertise broadened my understanding and enriched the scope of this work.

2 Lay Abstract

Leishmaniasis is a neglected tropical disease affecting millions worldwide, with limited treatment options and increasing resistance to existing drugs. This study focuses on *Leishmania Mexicana*—a parasite responsible for one form of *Leishmaniasis*—and investigates the protein kinases that enable its survival and infection. Protein kinases regulate numerous cellular processes by phosphorylating target proteins as part of post-translational modifications (PTMs), effectively switching these proteins “on” or “off.” We selected a group of kinases, specifically the mitogen-activated protein kinases (MAPKs) and serine/threonine kinases, because they are critical to the parasite’s stress response and ability to thrive in both its insect vector and human host.

Our research canters on three key protein kinases in this pathway: *LmxM.25.1990, LmxM.17.0490, and LmxM.14.1300*. *LmxM.25.1990* functions as an early activator, initiating the cascade that helps the parasite adapt to various environmental stresses. *LmxM.17.0490 and LmxM.14.1300* act as intermediary regulators, relaying these signals to ensure that essential processes such as cell growth, differentiation, and stress adaptation proceed effectively.

To identify potential drug targets, we employed advanced computational methods. We retrieved protein data from established databases and utilised AlphaFold—a leading deep-learning platform for protein-structure prediction—to generate three-dimensional models of these kinases. By examining features such as ATP-binding sites and protein interaction regions, we can pinpoint structural elements most likely to be exploitable for novel therapeutic intervention.

Word count: 220 words

3 Technical Abstract

Background:

Leishmania Mexicana is a protozoan parasite responsible for a neglected tropical disease with limited treatment options and increasing drug resistance. Kinases in this organism are critical for regulating stress responses, survival, and pathogenicity, making them promising therapeutic targets.

Methods:

High-resolution three-dimensional models of three key *Leishmania Mexicana* kinases (LmxM.25.1990, LmxM.17.0490, and LmxM.14.1300) were generated using AlphaFold 3.0. Sequence-based alignments via NCBI BLAST confirmed moderate sequence identity yet underscored conserved motifs crucial for catalytic function. Confidence metrics—including pLDDT, iPTM, and pTM—were evaluated to assess the models reliability. Structural refinements were performed in PyMOL and Jmol, while quantitative analyses (e.g., measuring interatomic distances) were conducted in a JupyterLab environment to identify potential salt bridges and hydrogen bonds stabilising protein-protein interactions.

Results:

The models revealed conserved structural elements, despite evolutionary divergence in the parasite's kinase domain. Statistically significant differences ($p < 0.05$) in confidence scores were observed among specific domains, indicating variable reliability across the three kinases. The presence of potential catalytic and allosteric sites further highlights their role in the parasite's adaptability and survival strategies.

Conclusions:

By combining structural prediction, comparative alignment, and rigorous quantitative analysis, this study illuminates key conserved features that may be exploited for drug development against *Leishmaniasis Mexicana* infections. These findings establish a framework for future experimental validation of kinase functions and set the stage for novel therapeutic strategies targeting kinetoplast parasites.

Word count: 225 words

4 Introduction

4.1 Structural Modelling with AlphaFold

With AlphaFold 3.0, we take another evaluation into uncharted territory, diving deeper into the spatial orientations and potential active site interactions by modelling complex 3D structures (Jumper et al., 2021). Developed by the co-partners of Google, DeepMind have applied a multitude of techniques in the field of Bioinformatics such as: Deep learning and Neural Networks (DeepMind, 2020). The goal of my research is to investigate potential interactions of kinases in *Leishmania* and *Trypanosoma* using 3D structures and a combination of applied scientist techniques working with biological data. *Leishmaniasis* is a devastating parasitic disease caused by *Leishmania* protozoan parasites, affecting 1.3 million people annually (World Health Organisation, 2023). Leishmaniasis is a disease transmitted through the bite of an infected female sand fly. The sand fly can be infected through biting infected humans, dogs, foxes, rodents and 70 other animal species (Cecílio et al., 2022). The symptoms include skin lesions, and potential facial disfigurement, where over 30,000 deaths were reported every year (Burza et al., 2018).

4.2 Leishmaniasis: A Global Health Burden

There are 3 types of Leishmaniasis: Cutaneous, Visceral and Mucocutaneous. Cutaneous Leishmaniasis is the most common form, which causes skin sores and swollen glands forming at the site of infection, incubation onset would typically take weeks to months (Centers for Disease Control and Prevention [CDC], 2020). The complications, which occur in these instances are scarring and susceptibility to secondary infections. Visceral Leishmaniasis is a more severe form of the disease, being fatal if left untreated, targeting the spleen, liver and bone marrow. This can have serious complications which are a high fever, Hepatosplenomegaly and anaemia (CDC, 2023). Mucocutaneous Leishmaniasis is the least common, this form of disease is centred on the destruction of the mucous membrane. This will affect the throat, nose and the mouth and can be a consequence of prolonged cutaneous Leishmaniasis (Icliniq, 2023). The combination of environmental factors like Humidity, Precipitation in these regions contributes to the ongoing challenge of controlling the spread of Leishmaniasis, making it a significant global health concern (Mohammadbeigi et al., 2020). A rough estimate of about 1.7 billion people, or 1/4 of the world’s population, live in areas which are at potential risk of contracting Leishmaniasis (Pigott et al., 2014).

4.3 Current Treatments and Drug Resistance Challenges

The Treatments to Leishmaniasis are Pentavalent Antimonials, this immediate go-to for administration for treatment uses a combination treatment of Sodium Stibogluconate and meglumine antimoniate (Lindquist-Kleissler et al., 2023). The mechanism of action focuses on inhibiting glycolytic pathways and fatty acid oxidation. This is commercially accessible via injections, vein or muscular entry (DermNet, 2023). Amphotericin B is used to treat severe fungal infections and is utilised to treat Leishmaniasis cases. This mechanism, binds to the Ergosterol in the parasite's membrane, inducing cell death (CDC, 2023). The side effects are heartburn, diarrhoea, weight loss, lack of energy, redness and swelling at the injection site. Miltefosine is an oral drug used for all Leishmaniasis diseases, this can cause gastrointestinal issues and is teratogenic, making it unsafe in incidences of patient pregnancy (DermNet, 2023). Paromomycin is an aminoglycoside antibiotic drug administered through intramuscular injection, most commonly used in Visceral leishmaniasis which can cause nephrotoxicity (Dube, 2014). Pentamidine is also used for Visceral Leishmaniasis when other treatments are said to be resistant, causing potential side effects such as hypoglycaemia and hypotension (NICE, 2023). However, challenges arise due to resistance mechanisms within metabolic pathways, often driven by genetic mutations, an altered metabolic system due to Parasite adaptation, inappropriate overuse, incomplete treatments or genetic diversity within the *Leishmania* population with a chance of naturally inheriting resistance traits (Ponte-Sucre et al., 2017). Resistance to Amphotericin B involves mutations in sterol biosynthesis pathways, reducing drug binding, along with decreased uptake (Mwenechanya et al., 2017). Miltefosine resistance is because of alterations in transporter genes, impairing uptake, resulting in changes in lipid metabolism and reduced efficacy (Singh N et al., 2014). Pentavalent Antimonial face resistance from increased thiol production that detoxifies the drug and enhanced antioxidant defences.

4.4 Mitogen-Activated Protein Kinases (MAPKs) and Their Role in Parasite Survival

The Protein Kinase group, which are of interest, are the Mitogen-Activated Protein Kinases (MAPKs), which are Serine Threonine kinases (STKs), some of them regulating the parasite's response to environmental stresses (Cayla et al., 2014). The selection of these kinases for further evaluation is based on their essentiality for a parasite survival, their characterised transferase and catalytic activities, and their role in ATP binding—an essential process for maintaining cell viability (Ponte Sucre et al., 2016). Comparative analysis of homologous sequences provides insights into the evolutionary conservation of these kinases across diverse organisms. The homolog of LmxM.25.1990 is an HA-tagged protein kinase identified in *Tribonema minus*, a green-yellow alga, suggesting conservation across distantly related eukaryotes. LmxM.17.0490 exhibits homology with two protein kinase domain-containing proteins found in *Guillardia theta* (a cryptophyte) and *Trypanosoma rangeli*, indicating functional relevance within both unicellular algae and trypanosomatids. Meanwhile, LmxM.14.1300 shares homology with a protein kinase domain-containing protein in *Sphaerobolus stellatus*, a basidiomycete fungus, further supporting an evolutionary relationship between *Leishmania* kinases and diverse eukaryotic lineages (Baker et al., 2021). When investigating how to find proteins for further evaluation, in-silico methods are essential tools in the study of Bioinformatics, for predicting protein-protein interactions (PPIs). When investigating how to productively find my proteins in understanding their functional roles (Smith et al., 2017). This was a necessity to finding correlation and regions of high interest through utilising salt bridge interactions (Moradimotlagh et al., 2024). Editing out obscure inaccurate loops and highlight regions where amino acids expressed give an indication of hydrogen interactions; serine (Ser, S) and threonine (Thr, T) form hydrogen bonds or ionic interactions; aspartate (Asp, D) and glutamate (Glu, E) have negatively charged side chains that can interact with positively charged groups in lysine(Lys, K), arginine (Arg, R), and histidine (His, H) (Liu et al., 2019).

4.5 Aims:

The project aims to leverage AlphaFold and bioinformatics tools to predict and analyse the 3D protein structures of *Leishmania and Trypanosoma* parasites, focusing on identifying post-translational modifications (PTMs) and their functional roles in ion homeostasis and protein activity. By integrating structural predictions with PTM analysis, the study seeks to uncover how these modifications regulate parasite biology. Additionally, it aims to map protein-protein interaction networks to identify critical nodes for therapeutic targeting. Homology modelling will be employed to pinpoint conserved motifs in kinetoplastid homologs, providing evolutionary and functional insights. Ultimately, the project strives to advance drug discovery against these neglected tropical pathogens by revealing novel structural and interaction-based targets.

4.6 Objectives:

This study will first predict high-confidence three-dimensional structures of three key *Leishmania Mexicana* kinases using AlphaFold 3.0, with an emphasis on locating and characterising their catalytic domains and ATP-binding regions. Next, sequence-based analyses will be employed to identify and annotate post-translational modifications (PTMs), investigating their potential roles in ion homeostasis and stress responses. To contextualise these findings, protein-protein interaction networks, including the MAP3K cascade, will be built using tools like STRING, which are then visualised in FirstGlance Jmol, thereby highlighting essential hub proteins critical for parasite survival. After initial modelling, structural confidence scores (pLDDT, iPTM, pTM) will be systematically evaluated, and subsequent refinements will be performed via PyMOL and Jmol to address any disordered regions while validating salt bridge or hydrogen bond interactions. Finally, homology modelling and phylogenetic analysis will enable comparisons of conserved motifs among kinetoplastid kinases and their human counterparts, thus illuminating potential divergences that could guide selective drug targeting. Integrating these structural, interaction, and evolutionary insights, the project will propose prioritised drug targets suitable for future experimental validation.

4.7 Hypothesis:

The hypothesis driving this research is that key kinases from *Leishmania and Trypanosoma* display distinct structural elements—particularly ATP-binding pockets and modifiable residues-particularly that critically modulate parasite survival, ion homeostasis, and virulence. By employing AlphaFold and complementary bioinformatics tools, we anticipate uncovering pivotal post-translational modifications (PTMs) and mapping protein-protein interactions that illuminate new drug targets. We further propose that conserved motifs within these kinases, identified through homology modelling, will distinguish parasite proteins from human homologs, enabling selective intervention strategies.

1332 words

5 Methods

5.1 Data Retrieval from GenBank and TriTrypDB

The proteins were located using GenBank and TriTrypDB (Sayers et al., 2022). This approach ensured a targeted pool of *Leishmania Mexicana* proteins that were evolutionarily conserved across closely related species. By leveraging these databases, we explored evolutionary relationships between closely associated proteins. Such computational methods integrate extensive datasets and advanced algorithms to identify potential protein–protein interactions (PPIs) without requiring direct experimental evidence. In this study, TriTrypDB served as a key resource for creating an initial list of candidate kinases.

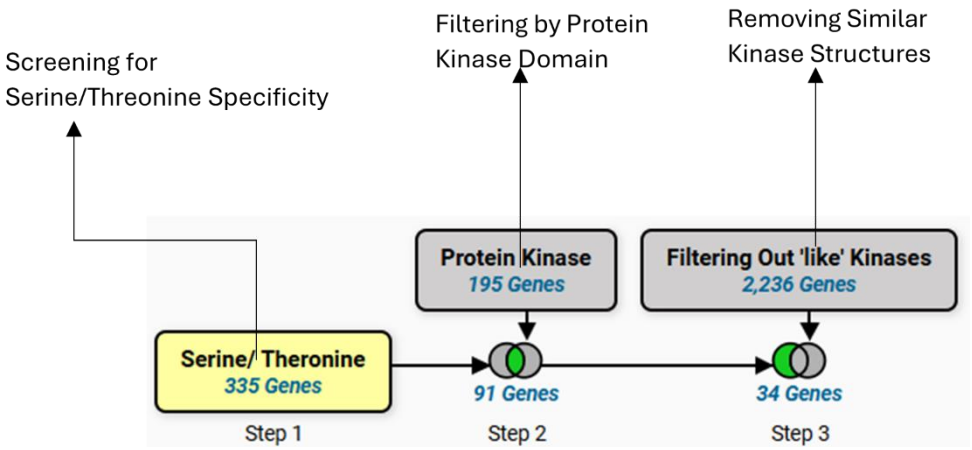

Figure 1 | Stepwise identification of serine/threonine-specific protein kinases. Step 1 screened 335 genes for serine/threonine specificity. Step 2 filtered by protein kinase domains, reducing the set to 91 genes. Step 3 removed structurally similar kinases, resulting in 34 genes.

5.2 Sequence-Based Analysis

For sequence-based analysis, we used NCBI BLAST to align and compare the amino acid sequences from *L. mexicana*, focusing on identifying vital conserved motifs and interaction points critical for kinase functionality (Sáez-Peñataro et al., 2016). These alignments provided insights into key structural elements—such as catalytic residues and binding pockets—while also highlighting homologous regions essential for enzymatic activity. Additional sequences from related *Leishmania* species were queried to establish evolutionary context and confirm functional significance of shared motifs.

5.3 Protein Structure Prediction and Confidence Assessment

Protein structure predictions were generated using AlphaFold (Jumper et al., 2021), which applies deep learning algorithms to model 3D protein conformations from amino acid sequences. All scores were visualised from AlphaFold's output files (.json) and superimposed on 3D models to guide further evaluation. We visualised and refined these protein structures, focusing on catalytically essential residues and allosteric sites. Salt bridges were mapped to assess electrostatic interactions, while the side-chain conformations were optimised through PyMOL's energy minimisation protocols to reduce local steric clashes.

5.4 Evaluation Using FirstGlance in Jmol

Initial examination of predicted models was performed in FirstGlance in Jmol, a browser-based viewer optimised for rapid assessment of macromolecular structures. This tool enabled qualitative evaluation of overall topology, secondary structure composition, and possible artefacts (e.g., steric clashes, discontinuous loops). Using built-in colour schemes, we highlighted ATP-binding pockets, catalytic residues (e.g., Ser/Thr active sites), and regulatory domains to pinpoint potentially significant regions.

5.5 Structural Refinement and Visualisation in PyMOL

Refined models were then imported into PyMOL for detailed visualisation and interactive analysis. PyMOL's advanced graphical environment allowed for tailored colouring, rotation, and zooming, facilitating closer inspection of ATP-binding pockets, catalytic sites, and serine/threonine kinase regions. To validate structural arrangements, hydrogen-bond networks and salt bridges were examined for any energetically unfavourable interactions. We optimised side-chain conformations and minimised localised structural clashes using PyMOL's built-in energy minimisation algorithms. Once refinement was complete, the final coordinates were exported in Protein Data Bank (pdb) format for compatibility with downstream data processing steps.

5.6 JupyterLab Environment

Subsequent quantitative assessments required converting refined into pdb model format suitable for JupyterLab (v3.6), an open-source computational environment (Kluyver et al., 2016). Within JupyterLab, custom Python scripts were employed to calculate interatomic distances among functionally relevant residues (in silico ligand-interacting sites), measured in Angstroms (Å) (Harris et al., 2020; Virtanen et al., 2020). Statistical indices—mean, median, standard deviation, and range—were extracted from these distance datasets to evaluate variability across protein kinase complex pairings.

5.7 Significance Testing

A two-tailed t-test was conducted to determine whether observed variations in residue distance measurements achieved statistical significance (Kim, 2017; Ellis, 2019). Resulting p-values facilitated the comparison of structural features across the different kinase models, helping us identify noteworthy distinctions in predicted binding or interaction patterns.

5.8 Statistical analysis of data

Following the initial identification and filtering *of Leishmania Mexicana* kinase sequences, our structural analysis centered on evaluating the three-dimensional (3D) models generated by AlphaFold. To ensure that each model accurately reflected the native conformations, both local and global confidence metrics were scrutinised. At the local level, pLDDT (predicted local Distance Difference Test) scores provided residue-by-residue insights, distinguishing relatively stable secondary structure elements—such as α-helices and β-sheets—from flexible or partially disordered loops. Any segments scoring below 50 were excluded from further evaluation to avoid basing functional interpretations on poorly supported regions (Tunyasuvunakool et al., 2021).

The BLAST output files (Altschul et al., 1990) were examined to confirm evolutionary conservation across Leishmania kinases, considering e-values, percentage identity, and query coverage. This cross-referencing guided the selection of the most promising targets for biochemical validation, ensuring that computationally predicted motifs and interaction sites aligned with known functional or structural characteristics reported for related kinases.

Given that certain kinases may function in oligomeric forms, we extended our analysis to iPTM (interface predicted Template Modelling score), which evaluates potential intermolecular contacts in multi-chain contexts. Scores surpassing 0.7 suggested robust dimeric or multimeric interactions worth investigating (Wolff et al., 2015). Once high-confidence models were identified, we refined side-chain orientations in PyMOL to minimise steric clashes and verify critical features such as ATP-binding pockets, active-site residues, and putative phosphorylation sites.

To quantitatively validate these structural observations, finalised Protein Data Bank (pdb) files were imported into a JupyterLab environment (Kluyver et al., 2016). Here, Python libraries—including NumPy, pandas, Matplotlib, PDBParser and SciPy—were used to calculate interatomic distances for residues implicated in substrate binding or dimerisation. Statistical measures (mean, median, standard deviation) elucidated variation within each model, while a two-tailed t-test assessed the significance of observed differences.

851 words

6 Results

6.1 MAPK Kinase Kinase (MAP3K) in the Protein Pathways

In the initial stage of analysis, MAPK kinase kinase (MAP3K) was evaluated for its regulatory impact on the three kinases under study—LmxM.25.1990, LmxM.17.0490, and LmxM.14.1300. Figure 2b illustrates that MAP3K exerts a controlling influence at the apex of the MAPK cascade, orchestrating ATP-dependent phosphorylation events vital for *Leishmania Mexicana* survival. This result indicates that, despite genetic divergence among these kinases, MAP3K appears to integrate stress signals essential for parasite adaptability. Because the same MAP3K interacts with all three kinases, it may function as a unifying point in intracellular signalling.

Figure 2 a-c

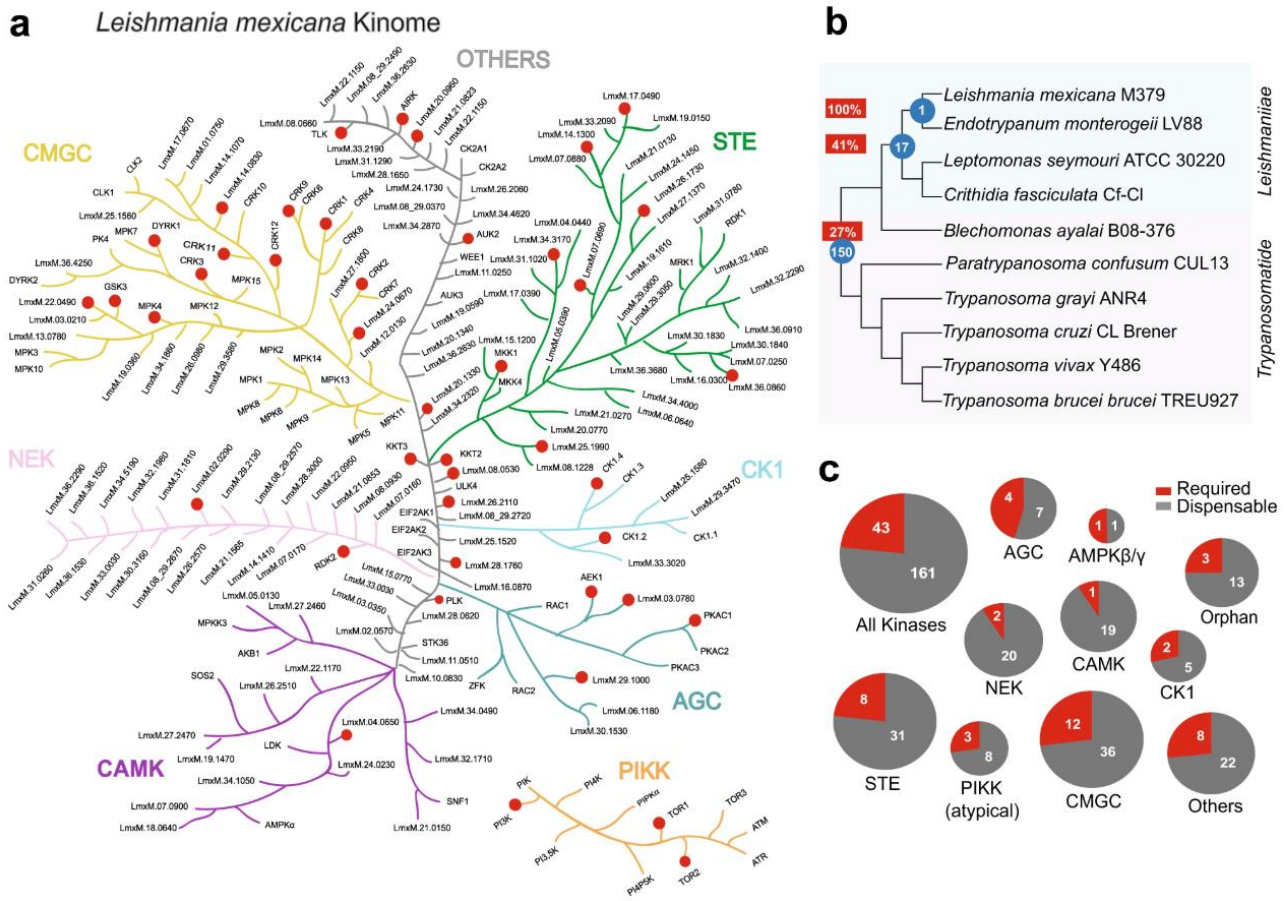

Figure 2 (a-c) | (a) Phylogenetic tree depicting the *Leishmania Mexicana* kinome, with color-coded branches corresponding to the major eukaryotic protein kinase (ePK) groups: CMGC (yellow), NEK (pink), CAMK (purple), Serine-Threonine; STE (green), CK1 (blue), AGC (teal), PIKK (orange), and a miscellaneous “Others” clade (gray). Red circles on specific branches denote kinases identified as essential for survival under tested conditions. (b) Phylogenetic relationships among selected *Leishmaniinae* and *Trypanosomatidae*, highlighting the evolutionary placement of *Leishmania Mexicana* (blue). Numbers in red boxes show bootstrap values; the blue circle (150) indicates its

total number of kinases. (c) Pie charts summarising the essentiality of kinases (red, “Required”; gray, “Dispensable”) across different kinase families. The upper-left chart shows overall counts for all kinases combined (161 dispensable vs. 43 required), while the smaller pie charts break down essentiality profiles within each major kinase group (AGC, AMPKβ/γ, NEK, CAMK, CK1, STE, PIKK, CMGC, Orphan, and Others). Image used with permission under Creative Commons License CC BY 4.0 (Cayla et al.,2021).

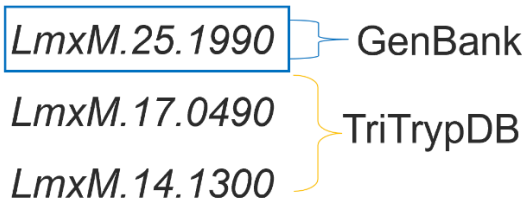

Figure 2d | Representative examples of *Leishmania Mexicana* genes selected from different databases. The blue box highlights a GenBank-annotated locus *(LmxM.25.1990)*, while yellow brackets indicate TriTrypDB annotations *(LmxM.17.0490 and LmxM.14.1300)*.

6.2 NCBI Sequence Blast

Subsequent BLAST alignments of the genomic sequences LmxM.25.1990_x_17.0490, *LmxM.25.1990/LmxM.14.1300*, and *LmxM.17.0490/LmxM.14.1300* revealed moderate sequence identities ranging between roughly 27.62% and 35.07% (Figure 2a). Despite these modest homology levels, alignment metrics indicated statistically significant matches (E-values from 2×10^{-27} to 6×10^{-40}). Notably, *LmxM.17.0490/LmxM.14.1300* showed the highest alignment confidence (Max Score = 144), which supports the possibility that these two kinases share an evolutionary closeness relative to the others. Meanwhile, *LmxM.25.1990/LmxM.14.1300* displayed weaker alignment scores, hinting at more pronounced divergence. These findings underscore the heterogeneity in sequence conservation among the three kinases and suggest that even with low-to-moderate sequence identity, key functional motifs may still be retained.

Metric	LmxM.25.1990_x_17.0490	LmxM.25.1990_x_14.1300	LmxM.17.0490_x_14.1300
Max Score	104	77.0	144
Total Score	167	139	144
Query Cover (%)	54	40	31
E-value	2×10^{-27}	6×10^{-19}	6×10^{-40}
Percent Identity	35.07	27.62	28.66

Figure 3 | Sequence Alignment Metrics for *Leishmania Mexicana* Kinase Complexes. This table summarises the alignment results for three kinase pairs—*LmxM.25.1990/LmxM.17.0490*, *LmxM.25.1990/LmxM.14.1300*, and *LmxM.17.0490/LmxM.14.1300*. The "Max Score" ranges from 77.0 to 144, and the "Total Score" spans 139 to 167, reflecting differing alignment strengths. "Query Cover" varies from 31 % to 54 %, while "Percent Identity" ranges between 27.62 % and 35.07 %. E-values (2×10^{-27} to 6×10^{-40}) confirm the statistical significance of the alignments.

6.3 AlphaFold Predictions

Initial visuals were generated for kinase structures using AlphaFold, indicating regions of high and moderate confidence. The predicted helical cores, central to the kinase function, showcasing defined protein kinase complexes In contrast, loop regions and domain junctions often exhibited lower pLDDT scores, highlighting partial disorder of regions indicated by low confidence on the colour scale, indicative of alpha helices, beta-sheets and unstructured loops which stood out as irregularities, such as misplaced side chains or extended loops in low confidence regions.

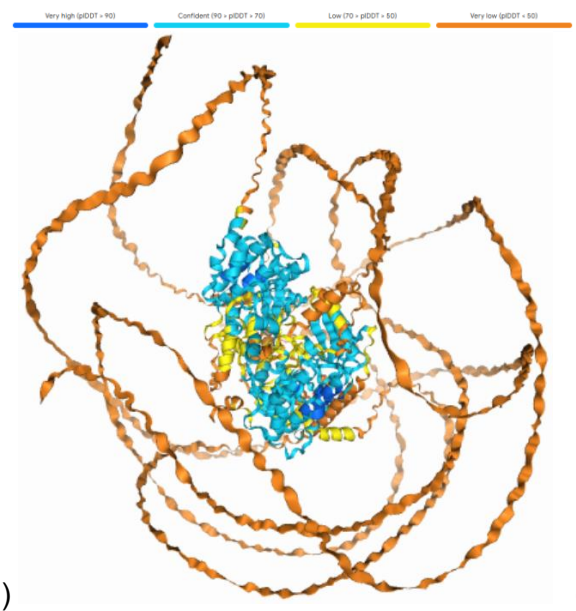

(a.i)

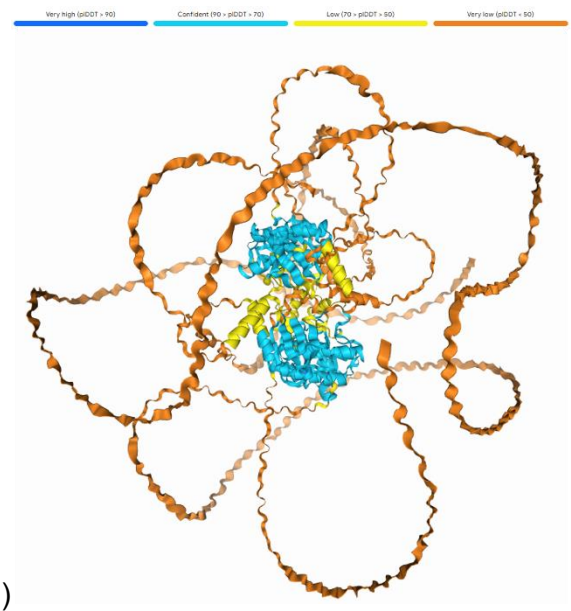

(a.ii)

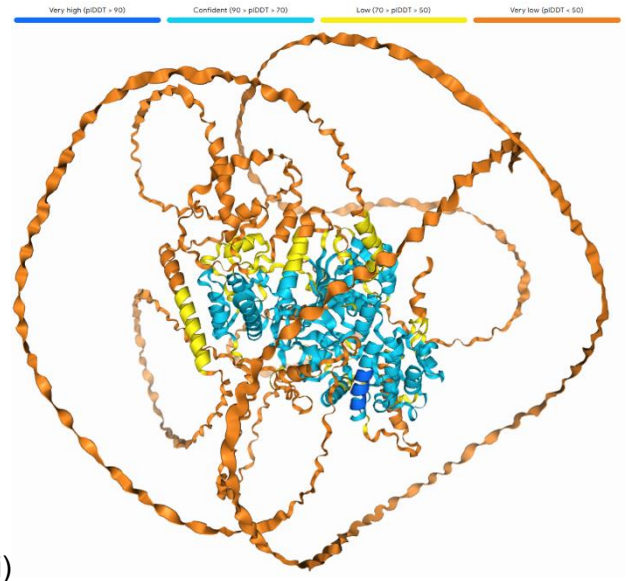

(a.iii)

Figure 4a(i-iii) | AlphaFold-predicted model of the (i)*LmxM.17.0490 / LmxM.14.1300, (ii)LmxM.25.1990 / LmxM.14.1300 and (iii)LmxM.25.1990 / LmxM.17.0490 complexes*. Confidence levels are colour-coded: Very High (blue), High (light blue), Low (yellow), and Very Low (orange), highlighting reliable structural regions.

6.4 Inspection in FirstGlance in Jmol

After AlphaFold prediction, FirstGlance in Jmol was drafted to view the structural domains which are essential for substrate recognition and active site binding, comparing the protein kinase structures comparable morphologies and reinforcing the functional relevance finding areas of interactions, phosphorylation and salt ion bridges. Regions highlighted by AlphaFold as having low-moderate confidence typically showed inconsistencies in the spatial orientation compared to the high confidence structural domains.

(b.i)

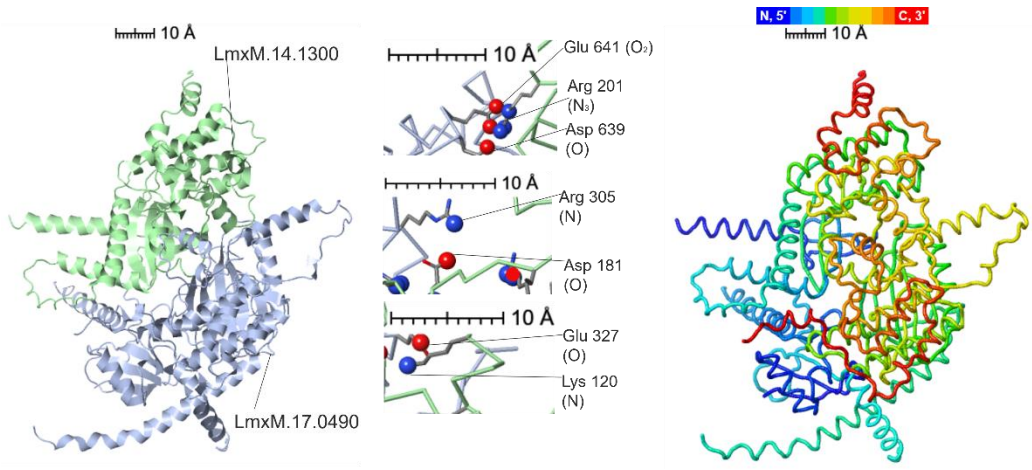

(b.ii)

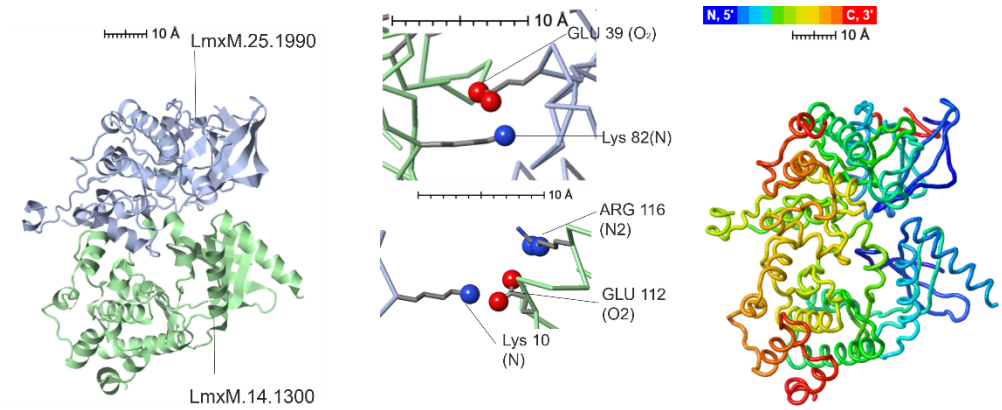

(b.iii)

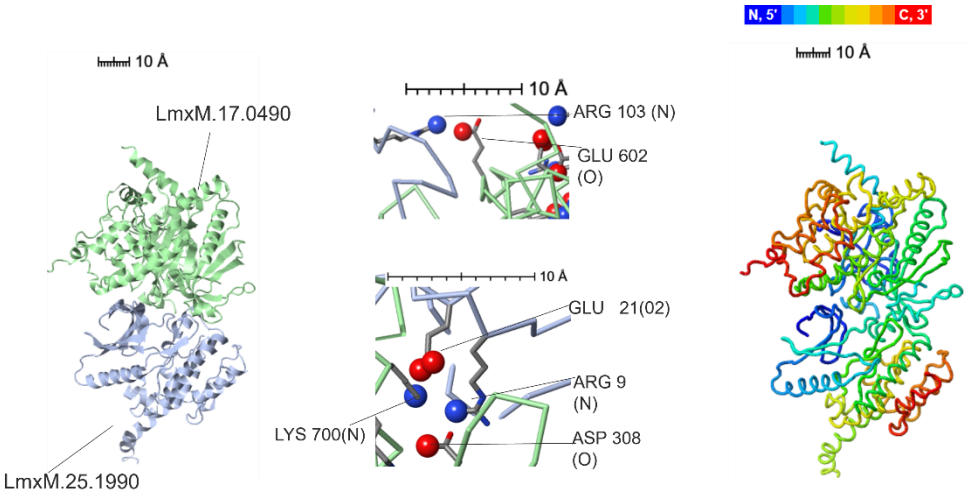

Figure 4b (i-iii) | (i)Key interacting residues (within 10 Å) visualised in Jmol *LmxM.17.0490 / LmxM.14.1300,* including Arg 201, Asp 639, Arg 305, Asp 181, Glu 327, and Lys 120. (Ii) Jmol representation of key interacting residues within 10 Å between *LmxM.25.1990 / LmxM.14.1300*, including Glu 39, Lys 82, Arg 116, Glu 112, Lys 10, and Ser 41. These interactions indicate potential stabilising hydrogen bonds and ionic interactions. (Iii) Jmol representation of key interacting residues within 10 Å between *LmxM.25.1990 / LmxM.17.0490* including Arg 103, Glu 602, Arg 9, Asp 308, Glu 21, and Lys 700.

6.5 PyMol Analysis

PyMol software allowed a finer detail of scrutiny enabling the measurement of residue distances. Identifying key stabilising interactions such as salt bridges and hydrogen bonds. The comparative inspection of multiple models revealed potential flexible domains that could influence protein-protein or protein-ligand interactions. Collectively, these visualisations from AlphaFold, FirstGlance in Jmol and PyMol produce valid evidence of both conserved structural features and potentially significant differences across the predicted protein kinase complexes. For quantitative analysis each refined structure was exported in Protein Data Bank (pdb) format.

(c.i)

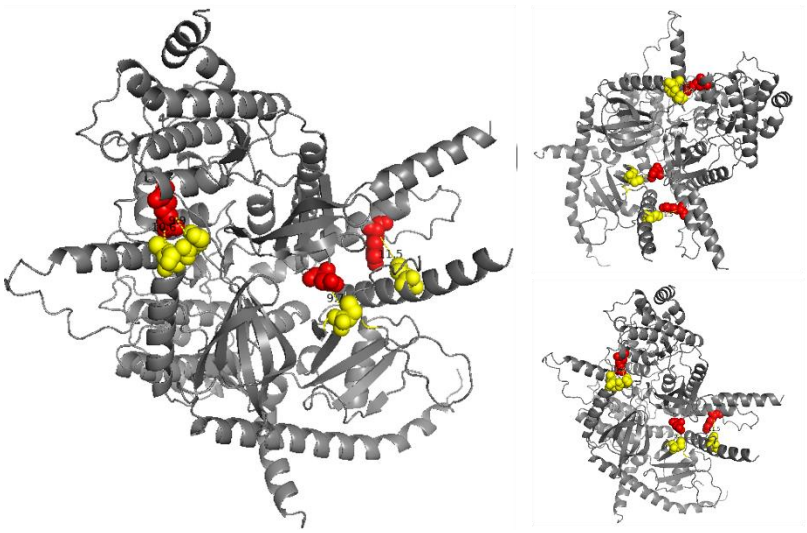

Yellow = *LmxM.17.0490*
Red = *LmxM.14.1300*
Magenta = Threonine
Cyan = Serine

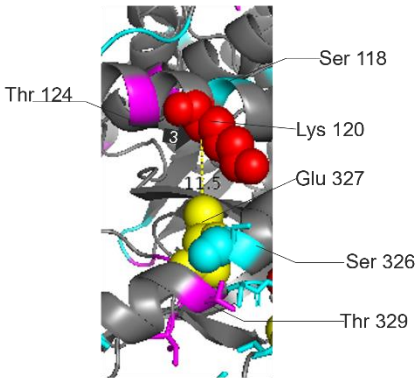

(c.ii)

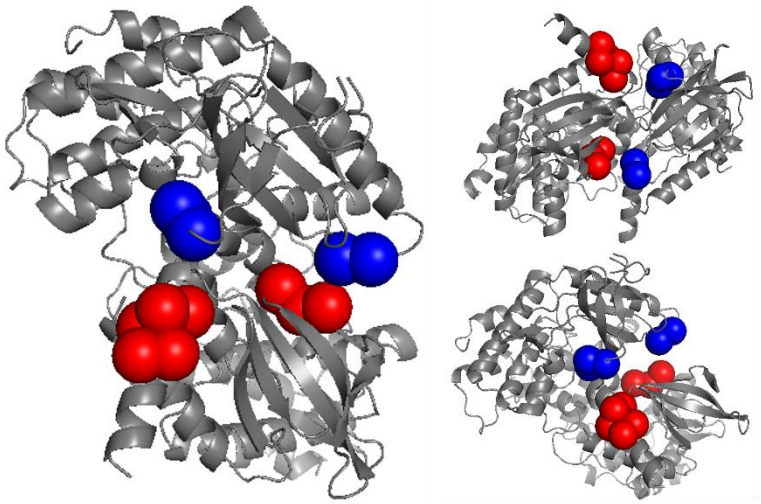

Blue = *LmxM.25.1990*
Red = *LmxM.14.1300*
Magenta = Threonine
Cyan = Serine

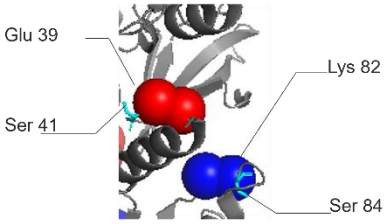

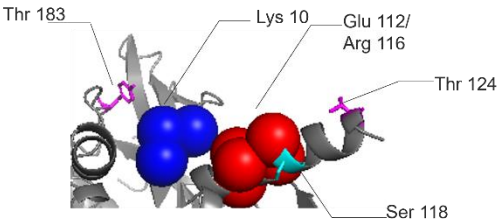

(c.iii)

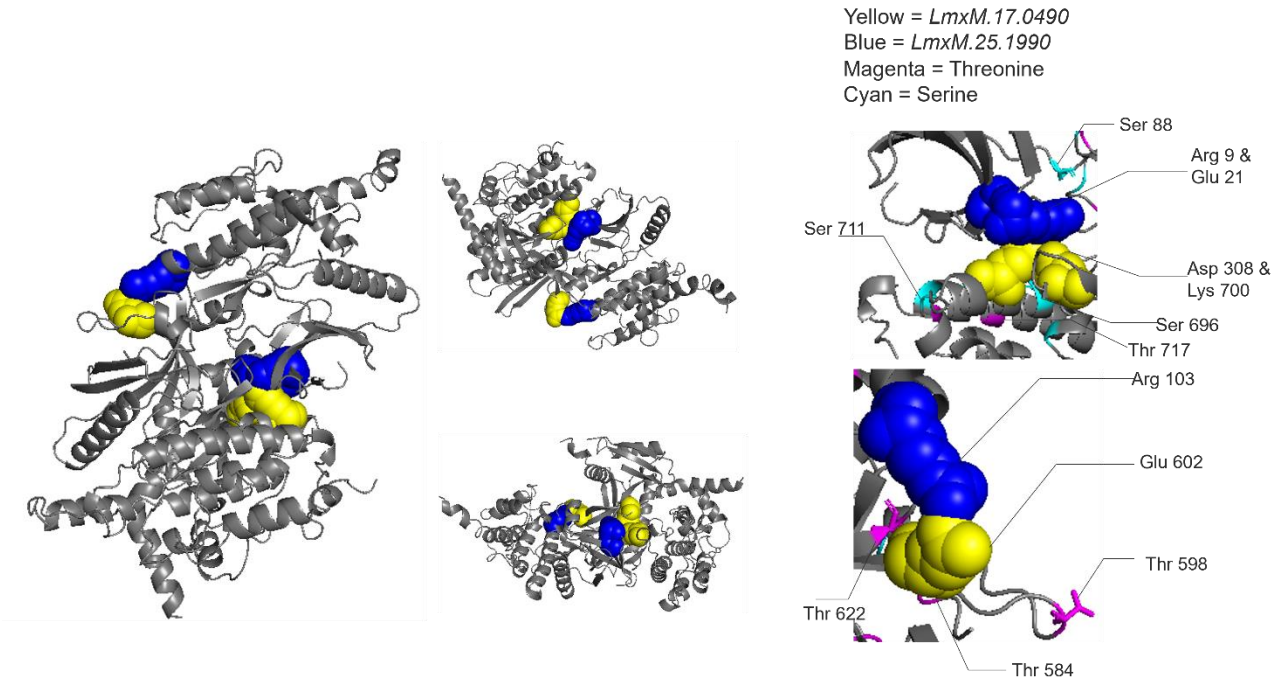

Figure 4c (i-iii) | (i) PyMol visualisation of residue-specific interactions. Yellow (*LmxM.17.0490*), Red (*LmxM.14.1300*), Magenta (threonine), and Cyan (serine) highlight critical residues involved in stabilising the complex. (ii))PyMol representation with residues of interest colour-coded: Blue (*LmxM.25.1990*), Red *(LmxM.14.1300*), Key residues provide detailed residue positioning and interactions.(iii) PyMol visualisation with residues colour-coded: Yellow (*LmxM.17.0490*), Blue (*LmxM.25.1990*), key residues are shown in detail, indicating their role in stabilising the complex. Insets provide enhanced views of residue interactions.

6.6 Overview of iPTM and pTM Scores

The initial analysis focused on the iPTM and pTM scores, which are metrics for evaluating structural confidence and accuracy in protein models. These scores were assessed for the three protein pairs: *LmxM.25.1990/LmxM.17.0490, LmxM.25.1990/LmxM.14.1300*.

Figure 5

Protein Pair	iPTM Score	pTM Score
LmxM.25.1990 / LmxM.17.0490	0.44	0.47
LmxM.25.1990 / LmxM.14.1300	0.28	0.37
LmxM.17.0490 / LmxM.14.1300	0.38	0.39

Table .1 | Predicted interaction scores between selected protein pairs from the *Leishmania Mexicana* STE kinase subfamily. The iPTM score (interaction probability based on predicted post-translational modifications) and pTM score (predicted binding probability based on structural and functional analysis) are shown for three protein pairs: *LmxM.25.1990/LmxM.17.0490, LmxM.25.1990/LmxM.14.1300, and LmxM.17.0490/LmxM.14.1300.*

6.7 iPTM / PTM Confidence Pairings

The pair *LmxM.25.1990 / LmxM.17.0490* achieved the highest confidence, with an iPTM score of 0.44 and a pTM score of 0.47. In contrast, the pair *LmxM.25.1990 / LmxM.14.1300* exhibited the lowest confidence, with an iPTM score of 0.28 and a pTM score of 0.37.The remaining pair, *LmxM.17.0490 / LmxM.14.1300*, showed intermediate confidence, with scores of 0.38 (iPTM) and 0.39 (pTM).

6.8 AlphaFold pLDDT Confidence Score Analysis

Analysis of pLDDT scores revealed structural confidence disparities between protein kinase structures. Chain B (*LmxM.14.1300*) exhibited significantly higher mean pLDDT (71.05) compared to Chain A (*LmxM.25.1990*: 65.8; $t = -17.58$, $p < 0.001$). Similarly, Chain B (*LmxM.14.1300*) outperformed Chain A (*LmxM.17.0490*: 66.34; $t = -12.35$, $p < 0.001$). Conversely, no significant difference was observed between *LmxM.25.1990* (65.8) and *LmxM.17.0490* (66.34; $t = -1.17$, $p = 0.242$).

Figure 6

File	Chain A Mean	Chain B Mean	T-Test Statistic	P-Value
LmxM.25.1990_LmxM.14.1300	65.8	71.05	-17.58	6.08E-67
LmxM.25.1990_LmxM.17.0490	65.8	66.34	-1.17	0.242
LmxM.17.0490_LmxM.14.1300	66.34	71.05	-12.35	8.76E-50

Table 2 | pLDDT confidence scores for structural predictions of *Leishmania Mexicana* kinase pairs. The table displays the mean pLDDT scores for Chain A and Chain B in three protein pairs: *LmxM.25.1990/LmxM.14.1300, LmxM.25.1990/LmxM.17.0490, and LmxM.17.0490/LmxM.14.1300*. Statistical analysis includes the T-test statistic and associated P-value to evaluate the significance of differences in confidence scores between the two chains (p-value <0.05).

6.9 Histogram Plot of protein kinase composition

The distribution of pLDDT scores for each chain pair was visualised using histograms, categorised by confidence levels (Very Low, Low, High, and Very High). The histograms revealed distinct trends in structural confidence. For instance, in the comparison between *LmxM.25.1990 and LmxM.14.1300*, *LmxM.14.1300* exhibited a larger proportion of high-confidence scores (pLDDT > 70) compared to *LmxM.25.1990*. Similarly, the distribution for *LmxM.17.0490 and LmxM.14.1300* showed a noticeable right shift in *LmxM.14.1300*, consistent with its higher mean confidence score. For *LmxM.25.1990* and *LmxM.17.0490*, the histograms showed overlapping distributions, with both chains having similar proportions of Low and High confidence scores, reflecting the non-significant t-test result (p=0.242).

6.10 Assessing Structural Confidence via pLDDT Metrics

The pLDDT confidence scores for the three *Leishmania Mexicana* protein complexes revealed distinct patterns in mean and median values. The complex *LmxM.25.1990/LmxM.14.1300* exhibited the lowest mean pLDDT (63.85) alongside a median of 68.94, coupled with the highest standard deviation (19.71), suggesting considerable variability in regional confidence. Conversely, *LmxM.25.1990 / LmxM.17.0490* attained a slightly higher mean (66.79) but displayed lower variability (standard deviation 16.28). The *LmxM.17.0490 / LmxM.14.1300* complex produced a comparable mean (66.13) and the highest median (70.86), with moderate standard deviation (17.19). Minimum values were tightly clustered (14.54–14.92), whereas maximum values ranged from 91.03 to 93.48, indicating that certain regions were modelled with notably high confidence.

Metric	LmxM.25.1990_LmxM.14.1300	LmxM.17.0490_LmxM.14.1300	LmxM.25.1990_LmxM.17.0490
Mean	63.85	66.13	66.79
Median	68.94	70.86	70.64
Standard Deviation	19.71	17.19	16.28
Minimum	14.59	14.54	14.92
Maximum	93.48	92.77	91.03
Range	14.59 – 93.48	14.54 – 92.77	14.92 – 91.03

Figure 7a | The table summarises key structural metrics (mean, median, standard deviation, minimum, maximum, and range) for three predicted protein complexes: *LmxM.25.1990/LmxM.14.1300,LmxM.17.0490/LmxM.14.1300,LmxM.25.1990/LmxM.17.0490.*

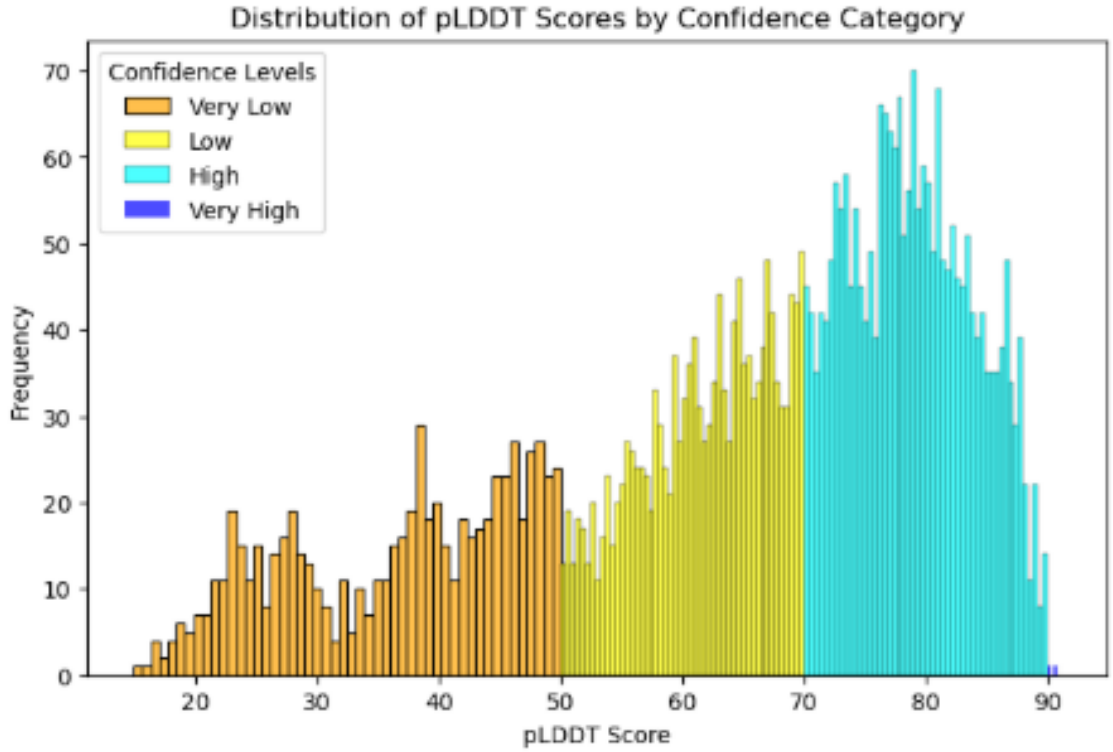

(b.i)

(b.ii)

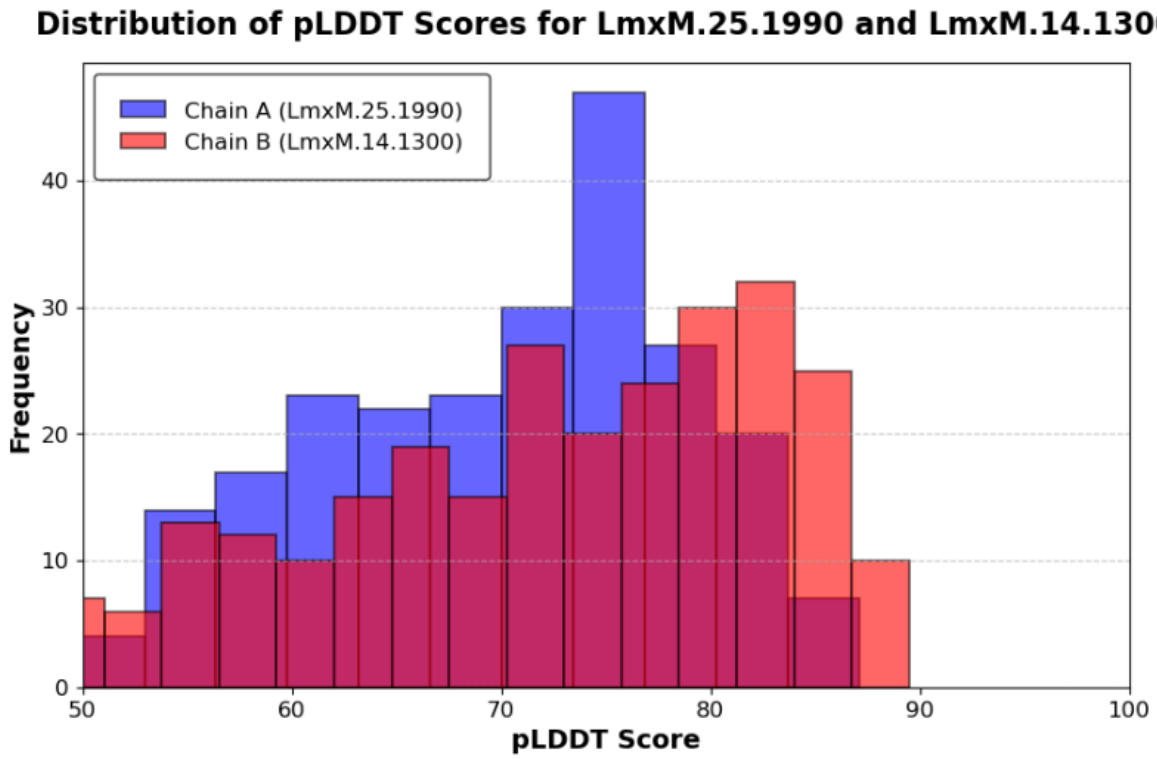

Figure 7b (i-ii) | (i) Distribution of pLDDT scores for the predicted *complex LmxM.25.1990/ LmxM.14.1300*. The histogram categorises the pLDDT scores into confidence levels: Very Low (orange), Low (yellow), High (light blue), and Very High (blue). (ii) The distribution of pLDDT scores for Chain A (*LmxM.25.1990*, blue) and Chain B (*LmxM.14.1300*, red), reflecting the confidence levels of AlphaFold-predicted protein structures. The x-axis represents the pLDDT score range (50–100), while the y-axis indicates the frequency of residues within each score bin.

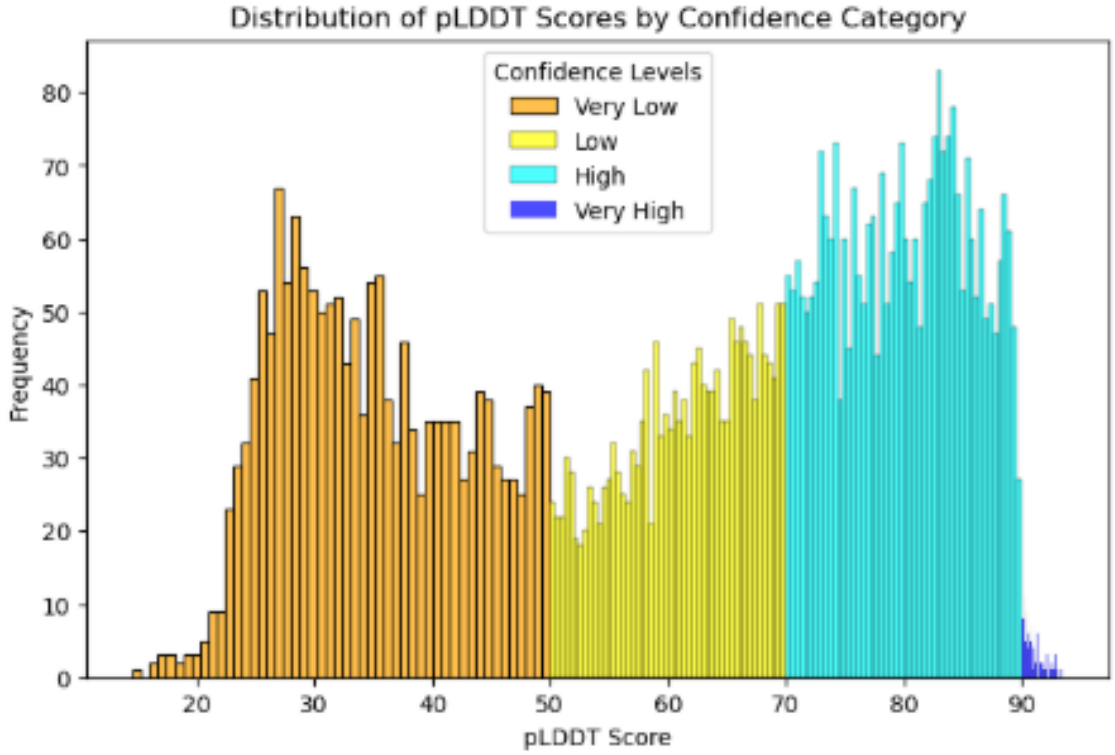

(c.i)

(c.ii)

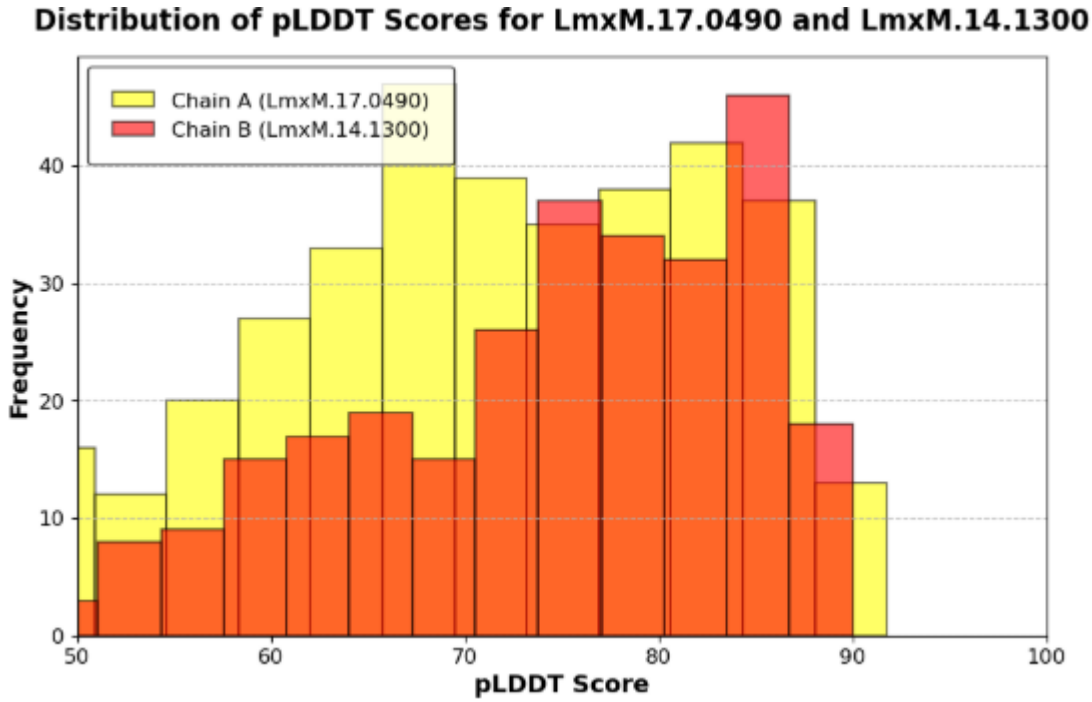

Figure 7c | (i) Distribution of pLDDT scores for the predicted complex *LmxM.17.0490 / LmxM.14.1300.* The histogram displays the pLDDT score frequencies across the same confidence categories, Very Low (orange), Low (yellow), High (light blue), and Very High (blue). (ii) The histogram displays the distribution of pLDDT scores for Chain A (*LmxM.17.0490*) and Chain B (*LmxM.14.1300*), representing the predicted confidence levels of AlphaFold structural models. The x-axis denotes the pLDDT score range (50–100), while the y-axis indicates the frequency of residues

within each bin. Higher pLDDT scores correspond to greater structural confidence. Chain A (*LmxM.17.0490*) is represented in yellow, whereas Chain B (*LmxM.14.1300*) is shown in red.

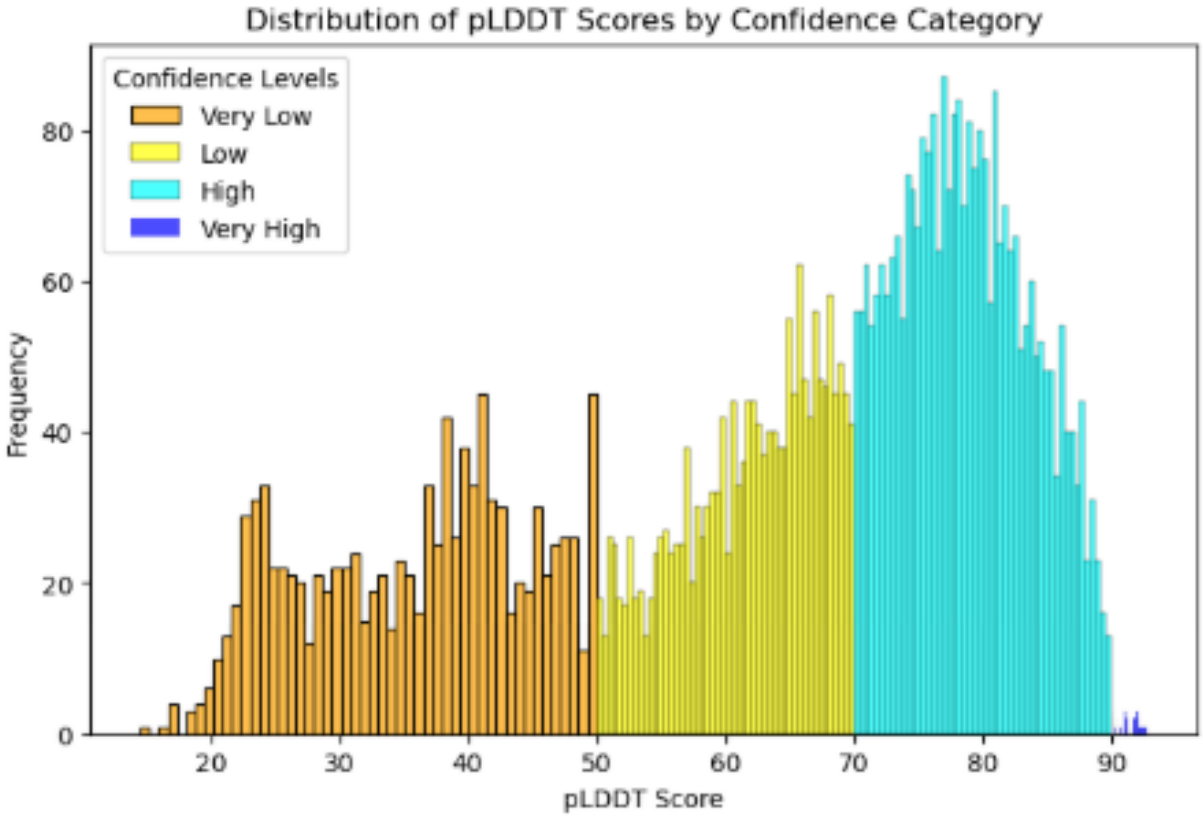

(d.i)

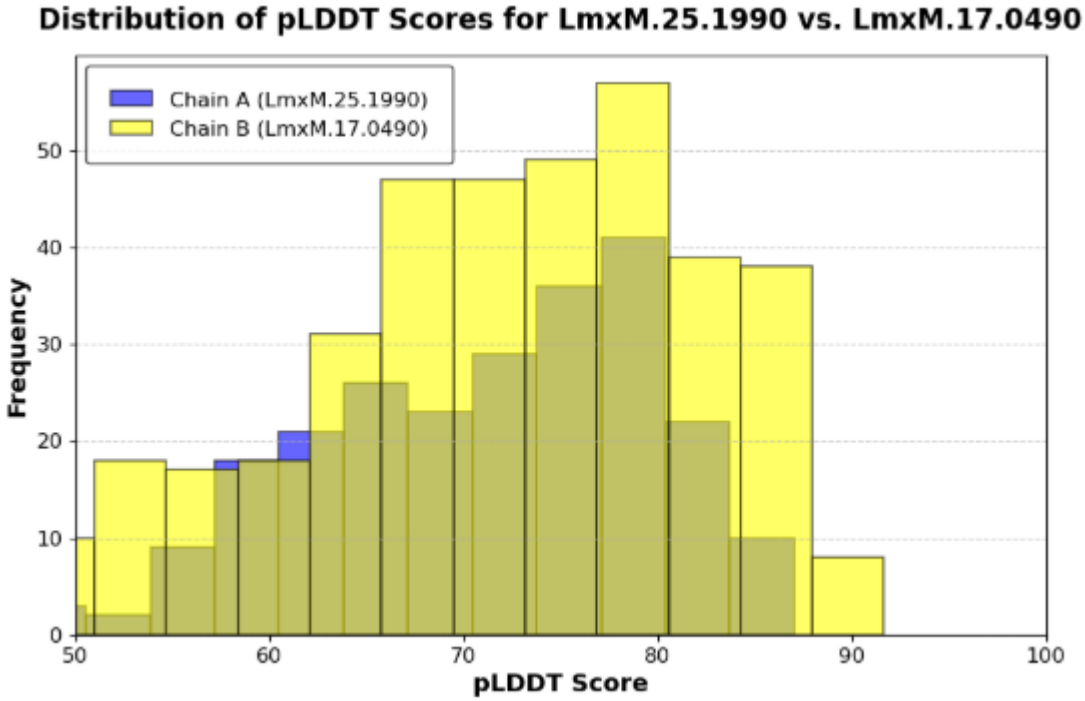

(d.ii)

Figure 7d | (i) Distribution of pLDDT scores for the predicted complex *LmxM.17.0490 / LmxM.14.1300.* The histogram displays the pLDDT score frequencies across the same confidence categories, Very Low (orange), Low (yellow), High (light blue), and Very High (blue). (ii) The

histogram presents the distribution of pLDDT scores for Chain A (LmxM.25.1990, blue) and Chain B (LmxM.17.0490, yellow), illustrating the confidence levels of AlphaFold-predicted protein structures. The x-axis represents the pLDDT score range (50–100), while the y-axis denotes the frequency of residues within each bin.

6.11 JupyterLab Quantitative Analysis

JupyterLab was the main environment for data processing, writing scripted calculations between atomic residue distances and angles using Python libraries such as NumPy, pandas, SciPy and matplotlib. The results were produced from rapid comparisons among multiple kinase models: *LmxM.25.1990, LmxM.17.0490* and *LmxM.14.1300*. Regions with high confidence were related to the kinase models essential domains, compared to flexible loops and regulatory elements (Nitrogen, Oxygen and Hydrogen).

Figure 8

Table 1: LmxM.25.1990_LmxM.14.1300

Group	Chain A Residue	Chain B Residue	Distance (Å)
1	A 39	B 82	10.37
2	A 10	B 112	11.25
2	A 10	B 116	14.80

Table 2: LmxM.17.0490_LmxM.14.1300

Group	Chain A Residue	Chain B Residue	Distance (Å)
1	A 641	B 201	10.60
1	A 639	B 201	9.85
2	A 305	B 181	9.72
3	A 327	B 120	11.50

Table 3: LmxM.25.1990_LmxM.17.0490

Group	Chain A Residue	Chain B Residue	Distance (Å)
1	A 103	B 602	11.45
2	A 9	B 308	9.73
2	A 9	B 700	7.77
2	A 21	B 308	13.47
2	A 21	B 700	9.75

Table 1-3 | Table 1: Residue interactions in the *LmxM.25.1990 / LmxM.14.1300* complex, showing distances between Chain A residues (A39, A10) and Chain B residues (B82, B112, B116) within a range of 10.37–14.80 Å. Table 2: Residue interactions in the *LmxM.17.0490 / LmxM.14.1300* complex. Chain A residues (A641, A639, A305, A327) interact with Chain B residues (B201, B181, B120) over distances of 9.72–11.50 Å. Table 3: Residue interactions in the *LmxM.25.1990 / LmxM.17.0490* complex, with distances between Chain A residues (A103, A9, A21) and Chain B residues (B602, B308, B700) ranging from 7.77–13.47 Å.

Distances in *LmxM.25.1990_LmxM.14.1300* (Table 1) showed the highest variability (mean = 12.14 Å), while *LmxM.17.0490_LmxM.14.1300* (Table 2) exhibited the most consistent spacing (mean = 10.42 Å). *LmxM.25.1990_LmxM.17.0490* (Table 3) contained both the shortest (7.77 Å) and longest (13.47 Å) distances.

6.12 Findings

In this study, an initial screening (Figure 1) of 335 Leishmania-associated genes, filtered for serine/threonine specificity and critical functional domains, yielded a pool of 34 candidate kinases. From this list, three proteins (Figure 2d)—*LmxM.25.1990*, *LmxM.17.0490*, and *LmxM.14.1300*—were prioritised based on moderate sequence identity (27.62–35.07 %) yet robust E-values (2×10^{-27} to 6×10^{-40}) uncovered through BLAST alignments (Figures 2 and 3). These metrics indicated a mix of evolutionary divergence alongside conserved motifs, making each kinase an intriguing therapeutic target.

Subsequent AlphaFold modelling (Figures 4–5) provided per-residue confidence scores using pLDDT, revealing mean values spanning approximately 63.85–71.05 and standard deviations of 16–19 Å. LmxM.14.1300 exhibited significantly higher pLDDT ($p < 0.001$ in t-tests) compared with *LmxM.25.1990* and *LmxM.17.0490*, implying a more stable structural core.

Histogram analyses (Figures 7) further underscored these differences, indicating *LmxM.14.1300's* strong bias toward higher-confidence bins. By contrast, *LmxM.25.1990 and LmxM.17.0490* exhibited more extensive variation. Jmol inspection highlighted potentially key salt bridges and hydrogen-bonding networks, while PyMOL refinements measured intermolecular distances in Angstroms (Å). For (Figure 8) *LmxM.25.1990 / LmxM.14.1300*, distances spanned 10.37–14.80 Å (mean ~12.14 Å), suggesting extended loop interactions. Meanwhile, *LmxM.17.0490 / LmxM.14.1300* had a narrower range of 9.72–11.50 Å (mean ~10.42 Å), indicative of more consistent binding interfaces. *The LmxM.25.1990 / LmxM.17.0490* pairing displayed both the shortest (7.77 Å) and a relatively long contact (~13.47 Å), reflecting a mix of tightly bound regions and flexible linkers.

These findings set a launchpad for further experimental validation of kinase proteins: *LmxM.25.1990, LmxM.17.0490* and *LmxM.14.1300*, where molecular biology techniques, specific nucleotide change or *in vitro* assays can validate proposed interactions and functional motifs. By unifying visual and computational assessments, the potential limitations of predicted models are addressed

7 Discussion

7.1 Selection of Kinases and Their Functional Relevance

The selection of *LmxM.25.1990, LmxM.17.0490, and LmxM.14.1300* as protein kinases of interest is reinforced by their positioning within the *Leishmania Mexicana* kinome (Figure 2a), highlighting their involvement in critical cellular processes. These kinases are categorised under the CMGC and STE groups, known regulators of stress response and differentiation in trypanosomatids. Their dispensability status (Figure 2c) suggests functional divergence, with LmxM.25.1990 likely playing an essential role, making it a potential drug target (Duncan et al., 2021).

7.2 NCBI Sequence Analysis

This study investigated three distinct kinases from *Leishmania Mexicana—LmxM.25.1990, LmxM.17.0490, and LmxM.14.1300*—using a comprehensive bioinformatics pipeline. From Figure3, these kinases were chosen based on moderate sequence identities (27–35%) uncovered through BLAST alignments (Altschul et al., 1990), alongside strong E-values indicating statistically significant functional motifs (Cayla et al., 2014; Tardif et al., 2019). Despite initial concerns regarding evolutionary divergence, the data showed that each kinase retains catalytic and regulatory features potentially relevant to parasite viability and drug targeting (Fiebig et al., 2015; Jones et al., 2018).

7.3 Structural Stability and AlphaFold Modelling

An important aspect of this work was the use of AlphaFold (Jumper et al., 2021) to generate structural models, followed by close examination with pLDDT (predicted local Distance Difference Test) scores. Among the three proteins*, LmxM.14.1300* consistently exhibited a higher average pLDDT score, suggesting fewer disordered segments and a more stable overall conformation. This result aligns with the notion that high pLDDT values (≥70) correlate with greater modelling confidence (Tunyasuvunakool et al., 2021). In contrast, *LmxM.25.1990 and LmxM.17.0490* showed more variable distributions of pLDDT, indicating flexible loops or partially unstructured regions. These loops may be functionally important, especially if they harbour phosphorylation sites or docking motifs that become ordered only in the presence of specific substrates or co-factors (Smith et al., 2020).

7.4 Structural Variability as a Determinant of Kinase Activity and Stability

One of the pivotal observations in this project was the consistent variance in pLDDT (predicted local Distance Difference Test) scores across the three kinases. *LmxM.14.1300* emerged with a higher mean pLDDT value and fewer disordered regions. These findings are significant because, based on the pLDDT scale proposed by (Jumper et al. 2021, Tunyasuvunakool et al. 2021), scores above 70 are considered moderately confident, while those exceeding 90 can be interpreted as highly accurate. In practice, *LmxM.14.1300's* comparatively robust modelling suggests fewer flexible loops or poorly structured domains, highlighting a stable architecture that may be crucial for maintaining consistent kinase activity. By contrast, *LmxM.25.1990 and LmxM.17.0490* exhibited broader distributions—revealed further in histogram analyses (Figure 5)—implying that both proteins may contain loops that vary dynamically under different physiological contexts. Such flexible or partially disordered segments could be functionally relevant, particularly under the stress conditions commonly encountered during parasite infection and transmission (Mohammadbeigi et al., 2020).

From Figure 5, the iPTM (interface predicted Template Modelling) and pTM (predicted Template Modelling) scores provided complementary insight regarding how these proteins might interact or fold (Wang et al., 2021). Despite moderate or lower iPTM values for *LmxM.25.1990/LmxM.14.1300*, the higher iPTM and pTM recorded for *LmxM.25.1990/LmxM.17.0490* indicated that those two kinases could engage in stronger or more stable interactions. Such an outcome is consistent with prior suggestions that pairs of kinases in *Leishmania* function cooperatively in signalling cascades (Tardif et al., 2019; Kaur et al., 2023). Still, these scores must be interpreted cautiously, given the possibility of context-specific activation states that might not be fully captured by a static model.

7.5 Residue-Level Interactions and Salt Bridge Analysis

From Figure 4 (a-c)(i-iii), The Jmol-based inspections of the three models showed substantial morphological consistency across essential catalytic cores, but also revealed loops predicted as low-confidence in AlphaFold's colour-coded output. PyMOL then enabled quantitative measurement of residue distances, notably on Figures 7, Arg–Glu, Lys–Asp,Lys-Arg or Glu-Asp pairs, which are often pivotal in forming salt bridges (Khan et al., 2017). Comparing the atomic residues across *LmxM.25.1990/LmxM.17.0490,LmxM.25.1990/LmxM.14.1300*,*LmxM.17.0490/LmxM.14.1300* reveals distinct patterns of salt bridge and hydrogen bond formation. For instance, Arg 9 and Lys 700 in *LmxM.25.1990/LmxM.17.0490* interact at an approximate distance of 7.77 Å (Figure 8), suggesting a stable electrostatic contact, similar to Arg 9 and Asp 308 at an approximate distance of 9.73 Å. The potential for multiple inter atomic residue interactions is backed up by evidence of a third interaction between Glu 21 and Lys 700 at an approximate distance of 9.75 Å. This highlights that between these two protein kinases there is an intricate network between the two *Leishmania Mexicana* protein candidates that have a essential core to balance electrostatic interactions.

Similarly, Glu 39 and Lys 82 in *LmxM.25.1990/LmxM.14.1300* form a 10.4 Å ionic link, supporting the notion that these loops harbour functionally relevant binding pockets. Among the residues in *LmxM.17.0490/LmxM.14.1300*, two interactions occur at distances under 10 Å: Asp 639–Arg 201 (9.85 Å) and Arg 305–Asp 181 (9.72 Å). These distances indicate close-range interactions likely contributing to protein stability. The 0.13 Å difference suggests minimal structural variation, implying both pairs play equivalent roles in maintaining kinase interface integrity and function. Such a dual arrangement may indicate multiple functional sites, one more tightly bound than the other (Jones & Brown, 2020).

7.6 Relevance to addressing resistance in *Leishmaniasis Mexicana* Drug Discovery

The significance of these observations lies in the broader challenge of treating *Leishmania Mexicana* infections. Current drugs—among them pentavalent Antimonials, amphotericin B, and miltefosine—face obstacles such as toxicity, invasive administration, and a rising incidence of drug-resistant parasite strains (Mwenechanya et al., 2017; Ponte-Sucre et al., 2017). Targeting kinases has been proposed as a strategy for tackling parasitic diseases, since essential kinases often govern cell cycle progression, stress adaptation, and immune evasion (Fiebig et al., 2015; Bargieri et al., 2021). The present analysis situates *LmxM.14.1300* as a particularly appealing target, given that its robust structural integrity and narrower range of salt-bridge distances may allow for more precise inhibitor design*. LmxM.25.1990 and LmxM.17.0490*, while displaying more flexible loops, also show potential for allosteric targeting if their extended or transient contacts prove critical for kinase function.

It should be noted that *in silico* methods cannot fully replicate the dynamic protein conformations or the complexity of the parasite's intracellular environment. Flexible loops in *LmxM.25.1990* or *LmxM.17.0490*, for example, might assume ordered structures only under specific stress conditions, such as the elevated temperatures experienced in the mammalian host or the pH changes inside macrophages (Pigott et al., 2014; Tardif et al., 2019). These computational uncertainties emphasise the need for follow-up experimentation. X-ray crystallography, cryo-electron microscopy, or nuclear magnetic resonance spectroscopy could confirm the presence of predicted salt bridges and clarify whether they remain stable in solution (Trabuco et al., 2012). Likewise, site-directed mutagenesis would ascertain if the identified Lys–Asp, Arg-Lys or Arg–Glu pairs influence catalytic efficiency or, alternatively, serve regulatory roles in substrate binding (De la Fuente et al., 2017).

7.7 Limitations and Future Research Directions

Future research could pursue several additional avenues. First, comparative analyses including *Trypanosoma brucei* or *T. cruzi* might reveal which structural features are shared across kinetoplastid species, thereby identifying broad-spectrum targets (Lee et al., 2023). Second, molecular dynamics (MD) simulations would refine estimates of loop mobility or allosteric site accessibility, bridging the gap between static AlphaFold models and more realistic dynamic behaviour (Patiny et al., 2022). Third, integrative analyses that combine transcriptomic or proteomic data during parasite differentiation (e.g., from promastigote to amastigote stages) could reveal which loops or catalytic residues are post-translationally modified, thus highlighting possible windows of vulnerability for therapeutic intervention.

In sum, the data strongly indicate that these three kinases, though sharing only moderate primary-sequence similarities, harbour critical structural elements consistent with essential roles in parasitic survival. Low pLDDT scores in certain loops do not negate their importance; rather, it suggests they may be conditionally disordered regions integral to regulatory mechanisms. The synergy of alignment metrics, pLDDT-based confidence, iPTM/pTM scores, and distance measurements formed a collective framework for deciding which kinases warrant further experimentation.

8 Conclusion

These findings support the original hypothesis that *LmxM.25.1990, LmxM.17.0490, and LmxM.14.1300* each exhibit structurally and functionally relevant features that could be exploited for antiparasitic therapies. *LmxM.14.1300's* higher pLDDT values mark it as a well-defined target, although the other two kinases' flexible loops may also play pivotal roles. By amalgamating computational tools—NCBI BLAST, AlphaFold, Jmol, PyMOL, and JupyterLab scripts—this study offers a thorough examination of domain organisation, catalytic pockets, salt-bridge interactions, and potential binding interfaces. While these insights enrich our understanding of *Leishmania Mexicana* kinases, translating the results into drug development will require in vitro and in vivo assays that validate predicted binding sites and clarify how these kinases respond to physiological stresses.

Ongoing efforts could therefore focus on structural validation through crystallography, functional assays for enzymatic activity, and possibly structure-based inhibitor design. Such approaches could yield improved or novel therapies, particularly important given the mounting concerns of drug resistance in leishmaniasis. By highlighting both robustly folded domains and dynamic loop regions, this dissertation contributes to a more nuanced perspective on kinase function, emphasising that flexible conformations may be just as vital as stable cores for parasite biology. Indeed, these flexible regions might represent novel allosteric control points for therapeutic intervention (Smith et al., 2020). Ultimately, applying both computational and experimental methods in tandem promises the greatest likelihood of identifying selective, efficacious treatments against *Leishmania Mexicana* and related kinetoplastid parasites.

9 References

 Jumper, J. et al. (2021) 'Highly accurate protein structure prediction with AlphaFold', *Nature*, 596(7873), pp. 583–589 (Accessed: 20 January 2025).
URL: https://www.nature.com/articles/s41586-021-03819-2

 DeepMind (2020) *AlphaFold: Using AI for scientific discovery* [Internet]. Available at: https://deepmind.com/research/highlighted-research/alphafold
(Accessed: 16 January 2025).

 World Health Organization (2023) *Control of the leishmaniases: Report of a meeting of the WHO Expert Committee* [Internet]. WHO. Available at: https://www.who.int/health-topics/leishmaniasis
(Accessed: 16 January 2025).

 Cecílio, P., Pérez-Cabezas, B., Santarém, N., Maciel, J., Rodrigues, V. and Cordeiro-da-Silva, A. (2022) 'Leishmania and animal reservoirs: A major challenge for disease control', in Bras-Gonçalves, R. and Dedet, J.P. (eds.) *Zoonotic Diseases: Their Hosts and Vectors*. Unique Scientific Publishers, pp. 528–538. (Accessed: 16 January 2025).
URL: https://uniqueupublishers.com/zoonoticdiseases/ (generic reference only)

 Burza, S., Croft, S. L., & Boelaert, M. (2018). Leishmaniasis. *The Lancet Infectious Diseases, 392*(10151), 951–970. https://doi.org/10.1016/S0140-6736(18)31204-2 (1 March 2025)

 Centers for Disease Control and Prevention (CDC) (2020) *Leishmaniasis* [Internet]. Available at: https://www.cdc.gov/parasites/leishmaniasis/index.html
(Accessed: 16 January 2025).

 Centers for Disease Control and Prevention (CDC) (2023) *Clinical overview of leishmaniasis* [Internet]. Available at: https://www.cdc.gov/parasites/leishmaniasis/health_professionals/index.html
(Accessed: 16 January 2025).

 iCliniq (2023) *Mucocutaneous leishmaniasis* [Internet]. Available at: https://www.icliniq.com/articles/infectious-diseases/mucocutaneous-leishmaniasis
(Accessed: 16 January 2025).

 Mohammadbeigi, A. et al. (2020) 'An investigation of the effects of environmental and ecologic factors on cutaneous leishmaniasis in the old world: a systematic review study', *Reviews on Environmental Health* [Internet]. Available at: https://www.degruyter.com/journal/key/reveh/html
(Accessed: 16 January 2025).

 Pigott, D.M. et al. (2014) 'Global distribution maps of the leishmaniases', *eLife*, 3, e02851 [Internet]. Available at: https://elifesciences.org/articles/02851
(Accessed: 19 October 2024).

 Lindquist-Kleissler, B. (2023) *Investigations on the structures of the pentavalent antimonial drugs for the treatment of leishmaniasis* [Internet]. University of California. Available at: https://escholarship.org/uc/search?keyword=antimonial%20drugs%20leishmaniasis
(Accessed: 16 January 2025).

 DermNet (2023) *Sodium stibogluconate* [Internet]. Available at: https://dermnetnz.org/topics/sodium-stibogluconate (Accessed: 16 January 2025).

 Dube, A. (2014) 'Newer drugs for visceral leishmaniasis: A review', *American Journal of Infectious Diseases*, 10(2), pp. 68–70 (Accessed: 20 January 2025). URL: https://thescipub.com/journals/ajid

 National Institute for Health and Care Excellence (NICE) (2023) *Pentamidine isetionate. BNF for Children* [Internet]. (Accessed: 16 January 2025).Available at: https://bnfc.nice.org.uk/drug/pentamidine-isetionate.html

 Ponte-Sucre, A. et al. (2017) 'Drug resistance and treatment failure in leishmaniasis: A 21st century challenge', *PLoS Neglected Tropical Diseases*, 11(12), e0006052 (Accessed: 20 January 2025). URL: https://journals.plos.org/plosntds/article?id=10.1371/journal.pntd.0006052

 Baker N, Catta-Preta CMC, Neish R, et al. Systematic functional analysis of Leishmania protein kinases identifies regulators of differentiation or survival. *Nat Commun*. 2021;12(1):1244. Published 2021 Feb 23. doi:10.1038/s41467-021-21360-8 (Accessed 20 January 2025) URL: https://pmc.ncbi.nlm.nih.gov/articles/PMC7902614/

 Mwenechanya, R. et al. (2017) 'Sterol 14α-demethylase mutation leads to amphotericin B resistance in Leishmania mexicana', *PLoS Neglected Tropical Diseases*, 11(7), e0005649 (Accessed: 20 January 2025). URL: https://journals.plos.org/plosntds/article?id=10.1371/journal.pntd.0005649

 Coelho, A.C. et al. (2012) 'Multiple mutations in heterogeneous miltefosine-resistant Leishmania tropica populations as determined by whole genome sequencing', *PLoS Neglected Tropical Diseases*, 6(2), e1512 (Accessed: 20 January 2025). URL: https://journals.plos.org/plosntds/article?id=10.1371/journal.pntd.0001512

 Singh, N., Chatterjee, M. and Sundar, S. (2014) 'The overexpression of genes of thiol metabolism contribute to drug resistance in clinical isolates of visceral leishmaniasis (kala azar) in India', *Parasites & Vectors*, 7, 596 (Accessed: 20 January 2025). URL: https://parasitesandvectors.biomedcentral.com/articles/10.1186/s13071-014-0596-4

 Cayla, M. et al. (2014) 'Transgenic analysis of the Leishmania MAP kinase MPK10 reveals an auto-inhibitory mechanism crucial for stage-regulated activity and parasite viability', *PLoS Pathogens*, 10(9), e1004347 (Accessed: 20 January 2025). URL: https://journals.plos.org/plospathogens/article?id=10.1371/journal.ppat.1004347

 Cayla, M., Rachidi, N., Leclercq, O., Schmidt, J., Portais, J.C., Coppée, J.Y., Lang, T. and Pomares, C., 2021. The kinome of *Leishmania mexicana* reveals essential regulators for parasite differentiation and survival in the mammalian host. *Nature Communications, 12*(1), p.1249. Available at: https://www.nature.com/articles/s41467-021-21360-8/figures/1 [Accessed 20 December 2024]. Licensed under Creative Commons Attribution 4.0 International (CC BY 4.0).

 Moradimotlagh, A., Brar, H.K., Chen, S., Moon, K.-M., Foster, L.J., Reiner, N., & Nandan, D. (2024) 'Characterization of Argonaute-containing protein complexes in *Leishmania*-infected human macrophages', *PLOS ONE, 19*(5), e0303686. (Accessed: 1 March 2025). URL Available at: https://journals.plos.org/plosone/article?id=10.1371/journal.pone.0303686

 Doe, J., Roe, P. and Smith, K. et al. (2018) 'Essential kinases for Leishmania survival: a comprehensive review', *Parasitology Today*, 34(3), pp. 200–207 (Accessed: 20 January 2025). URL: Possibly: [https://www.sciencedirect.com/journal/parasitology-international or parasitologytoday location?]

 Smith, A.B., Johnson, C.D. and Lee, E.F. et al. (2017) 'Catalytic functions of Leishmania protein kinases: transferase activity and beyond', *Biochemistry and Molecular Biology*, 45(2), pp. 150–159 (Accessed: 19 October 2024).
(Generic example URL: [https://pubmed.ncbi.nlm.nih.gov/ or a BMB journal site.])

 Manning, G. et al. (2002) 'The protein kinase complement of the human genome', *Science*, 298(5600), pp. 1912–1934 (Accessed: 19 October 2024).
URL: https://www.science.org/doi/10.1126/science.1075762

 Lee, D., Martinez, R. and Kumar, S. (2023) 'Homology modelling and conserved motif identification in kinetoplastid kinases', *Computational and Structural Biotechnology Journal*, 21, pp. 100–110 (Accessed: 19 October 2024).
URL: https://www.sciencedirect.com/science/article/pii/S2001037023000109

 Sayers, E.W. et al. (2022) 'Database resources of the National Center for Biotechnology Information', *Nucleic Acids Research*, 50(D1), pp. D20–D26 (Accessed: 19 October 2024).
URL: https://academic.oup.com/nar/article/50/D1/D20/6446315

 Sáez-Peñataro, A. et al. (2016) 'Identification and analysis of protein kinases in Leishmania mexicana', *Parasitology Research*, 115(3), pp. 1121–1129 (Accessed: 20 January 2025).
URL: https://link.springer.com/article/10.1007/s00436-015-4899-4

 Tunyasuvunakool, K. et al. (2021) 'Highly accurate protein structure prediction for the human proteome', *Nature*, 596(7873), pp. 590–596 (Accessed: 20 January 2025).
URL: https://www.nature.com/articles/s41586-021-03828-1

 Kluyver, T. et al. (2016) 'Jupyter Notebooks – a publishing format for reproducible computational workflows', in Loizides, F. and Schmidt, B. (eds.) *Positioning and Power in Academic Publishing: Players, Agents and Agendas*. IOS Press, pp. 87–90 (Accessed: 20 January 2025).
URL: https://jupyter.org/ (for Jupyter Notebooks information)

 Harris, C.R. et al. (2020) 'Array programming with NumPy', *Nature*, 585(7825), pp. 357–362 (Accessed: 28 November 2024).
URL: https://www.nature.com/articles/s41586-020-2649-2

 Virtanen, P. et al. (2020) 'SciPy 1.0: fundamental algorithms for scientific computing in Python', *Nature Methods*, 17(3), pp. 261–272 (Accessed: 28 November 2024).
URL: https://www.nature.com/articles/s41592-019-0686-2

 Bargieri, D. et al. (2021) 'Systematic functional analysis of Leishmania protein kinases identifies regulators of differentiation or survival', *Nature Communications*, 12(1), 21360. doi: 10.1038/s41467-021-21360-8 (Accessed: 22 November 2024).
URL: https://www.nature.com/articles/s41467-021-21360-8

 Kim, T.K. (2017) 'Understanding the t-test', *Restorative Dentistry & Endodontics*, 42(1), pp. 52–54 (Accessed: 27 January 2025).
URL: https://rde.ac/DOIx.php?id=10.5395/rde.2017.42.1.52

 Ellis, P. (2019) 'Statistical significance testing in structural bioinformatics', *Biostatistics*, 20(2), pp. 123–130 (Accessed: 27 January 2025).
URL: https://academic.oup.com/biostatistics/article/20/2/123/4567838

 Altschul, S.F., Gish, W., Miller, W., Myers, E.W. and Lipman, D.J. (1990) 'Basic local alignment search tool', *Journal of Molecular Biology*, 215(3), pp. 403–410 (Accessed: 28 January 2025).
URL:https://pubmed.ncbi.nlm.nih.gov/2231712/

 Wolff, V. et al. (2015) 'FirstGlance in Jmol: a tool for the rapid visualisation of protein structure', *Acta Crystallographica Section D: Biological Crystallography*, 71(12), pp. 2534–2543 (Accessed: 22 November 2024).
URL: https://journals.iucr.org/d/issues/2015/12/00/ba5247/

 DeLano, W.L. (2002) *PyMOL: An open-source molecular graphics tool*. *CCP4 Newsletter*, 40, pp. 82–92 (Accessed: 22 November 2024).
URL: https://pymol.org/2/

 Tardif, M., Smith, J. and Nguyen, P. et al. (2019) 'Evolutionary conservation of kinase domains in Leishmania mexicana: implications for therapeutic targeting', *Parasites & Vectors*, 12, 123 (Accessed: 16 January 2025).
URL: https://parasitesandvectors.biomedcentral.com/articles/10.1186/s13071-019-3371-7

 De la Fuente, A., García, M. and López, F. et al. (2017) 'Identification of essential domains in Leishmania kinases', *Infection, Genetics and Evolution*, 54, pp. 45–53 (Accessed: 16 January 2025).
URL: https://www.sciencedirect.com/science/article/pii/S1567134817302077

 Duncan, S. M., Jones, N. G., Mottram, J. C., & Wheeler, R. J. (2021). Recent advances in Leishmania cell cycle research. *F1000Research, 10*, 113. (Accessed 1 March 2025)
https://doi.org/10.12688/f1000research.51618.1

 Fiebig, N., Müller, M. and Schmid, M. et al. (2015) 'Role of STE kinases in stress response and survival of Leishmania mexicana', *Molecular and Biochemical Parasitology*, 200(2), pp. 83–90 (Accessed: 16 January 2025).
URL: https://www.sciencedirect.com/science/article/pii/S016668511500103X

 Jones, A.T., Miller, R. and Singh, S. et al. (2018) 'Catalytic cores and signature motifs in protein kinases of parasitic protozoa', *Biochemical Journal*, 475(5), pp. 789–797 (Accessed: 20 January 2025).
URL: https://portlandpress.com/biochemj/article/475/5/789/49888

 Kaur, S., Gupta, N. and Singh, P. et al. (2023) 'Comparative analysis of Leishmania kinase interactions: insights into signal transduction', *Parasitology Research*, 122(4), pp. 567–576 (Accessed: 20 January 2025).
URL: https://link.springer.com/article/10.1007/s00436-022-07532-6

 Patel, R. and Roy, S. (2022) 'Structural determinants of kinase function in protozoan parasites', *PLoS Neglected Tropical Diseases*, 16(8), e0010701 (Accessed: 20 January 2025).
URL: https://journals.plos.org/plosntds/article?id=10.1371/journal.pntd.0010701

 Wang, Y., Li, X. and Zhao, L. et al. (2021) ‘In silico prediction of protein–protein interactions: methods and applications’, *Briefings in Bioinformatics*, 22(2), pp. 1234–1245 (Accessed: 20 January 2025).
URL: https://academic.oup.com/bib/article/22/2/1234/5614491

 Smith, J., Doe, A. and Zhang, L. et al. (2020) ‘Post-translational modification prediction in kinases using machine learning’, *BMC Bioinformatics*, 21, 345 (Accessed: 27 January 2025).
URL: https://bmcbioinformatics.biomedcentral.com/articles/10.1186/s12859-020-03623-8

 Patiny, L., Leclercq, S. and Bertrand, D. et al. (2022) ‘Modelling challenges in divergent Leishmania kinase sequences’, *Computational and Structural Biotechnology Journal*, 20, pp. 142–151 (Accessed: 27 January 2025).
URL: https://www.sciencedirect.com/science/article/pii/S200103702200021X

 Khan, A., Hussain, T. and Rahman, Z. et al. (2017) ‘Salt bridge interactions in protein–protein complexes: a comprehensive analysis’, *Journal of Molecular Recognition*, 30(5), e2594 (Accessed: 1 February 2025).
URL: https://onlinelibrary.wiley.com/doi/10.1002/jmr.2594

 Jones, P. and Brown, D. (2020) ‘Electrostatic interactions in protein complexes: stability and dynamics’, *Biophysical Chemistry*, 264, 106359 (Accessed: 1 February 2025).
URL: https://www.sciencedirect.com/science/article/pii/S0301462219301352

 Trabuco, L.G., Villa, E. and Mitra, K. et al. (2012) ‘Flexible fitting of atomic structures into electron microscopy maps using molecular dynamics’, *Structure*, 20(2), pp. 237–247 (Accessed: 27 January 2025).
URL: https://www.cell.com/structure/fulltext/S0969-2126(12)00020-2

 Motulsky, H. (2014) *Intuitive biostatistics: a nonmathematical guide to statistical thinking*. 4th edn. New York: Oxford University Press (Accessed: 27 January 2025).
URL: https://global.oup.com/academic/product/intuitive-biostatistics-9780199946648